Low-dimensional neural dynamics of freely-moving walking and reaching

Alissa S Ling[1], Michael P Silvernagel[1], Stephen E Clarke[2], Elizabeth J Jun[4], Paul Nuyujukian[1,2,3,5,6], for the Brain Interfacing Laboratory

[1]Department of Electrical Engineering.
[2]Department of Bioengineering.
[3]Department of Neurosurgery.
[4]Department of Neuroscience.
[5]Wu Tsai Neurosciences Institute .
[6]Stanford Bio-X, Stanford University.

*Corresponding author(s). E-mail(s):
23_freely_reach_walk@pn.stanford.edu;
Contributing authors: aling96@stanford.edu; mpsilver@stanford.edu;
stclarke@stanford.edu; ejjun@stanford.edu;

Abstract

We address a long standing question: is the richness of neural activity is constrained by behavioral complexity? Low-dimensional neural dynamics of unconstrained reaching and walking have similar dimensionality and power spectrum, yet distinct, cyclical trajectories for walking and flipped trajectories for reaching. Similar behaviors with different complexity may operate in a common neural subspace but unfold differently.

4 claims

Keywords: freely moving, neural dynamics, low dimensional

Figure out how to quantifiably defend each claim

Motor systems neuroscience seeks to explain the neural mechanisms behind voluntary movement in the brain. Multichannel recording has revolutionized the field by enabling simultaneous access to hundreds of recorded neurons. Awake, behaving animal experiments have been crucial to advancing our understanding. Traditional investigations focus on isolated movement, i.e., reaching, while eliminating other body movements using physical restraint, allowing for tighter correlations between the measured behavior and brain activity. Multidimensional statistical estimation tools applied to these studies have uncovered relationships between population activity of neurons and behavior that cannot be seen on a single-neuron level or trial-averaged basis [1, 2]. This mathematical modeling has been validated across multiple brain regions [3] and mammalian species, such as mice, primates [1], and humans [4, 5]. Decades of constrained primate studies have uncovered information about how the motor cortex drives motor behavior using dimensionality reduction techniques, such as the possible dimensionality of the neural population structure [6], the form [7, 8], and the bounds of the low-dimensional neural subspace [9–11]. These findings have revealed rich, low dimensional neural dynamics suggestive of the mechanisms underlying these isolated movements [12–15]

However, growing theoretical [16, 17] and experimental [18–21] evidence challenge generalizability to ambulatory behavior, highlighting a knowledge gap in the mechanistic understanding of how the brain controls free movement. Consequently, a natural question arises: does the complexity of a behavior change the involvement and neural population structure of the motor cortex? To answer this question, we conducted studies of free behavior in an experimental rig that captures wireless neural data and its relationship to movement of full-body limb coordination [22].

We defined complexity as intentionality of performing a movement, and sought to answer how the context behind similar behaviors influences neural activity in M1. Thus, we compared the neural response of two similar unconstrained arm movements: arm swing while walking and arm reaching to food. Under these task conditions, unconstrained arm reaching is an effortful, directed movement towards a reward, whereas unconstrained walking is an innate, well-practiced behavior. We performed 3 analyses: comparing median firing rates on a trial-averaged basis, quantifying the neural dimensionality of each task, and analyzing neural population dynamics. This study provides insight on how the brain may control free movement and questions the limitation of constrained behavioral animal studies.

We captured hundreds of trials over multiple days of natural, free walking and reaching, time-synchronized with neural data in two adult male rhesus macaques. Fig 1b displays example kinematics for the swing, stance, and subsequent arm reach for Monkey C. Neural data was recorded from a 96-channel electrode array (Blackrock Microsystems, Salt Lake City, UT) implanted in M1 left arm cortical region for Monkey C and M1 right arm cortical region for Monkey U and wirelessly telemetered with a battery-powered transmitter (Cereplex W, Blackrock Microsystems, Salt Lake City, UT). Figure 1c and 1d show 1-1.5 second binned neural threshold crossing rasters for Monkeys C and U for the contralateral limb. Both rasters show modulation during 200 ms periods of swing (blue) and reach (pink) for the contralateral arm. Fig 1c and 1d also show the median firing rates sorted by the most active channel for each

condition. For both monkeys, the neural firing rates for the directed reach to food was higher than the swing period, suggesting that the motor cortex is more active during directed reaches.

We next quantified the complexity of neural activity for swing and reach by comparing the dimensionality and eigenspectra. Swing trials consisted of 200 ms periods from the beginning of the swing phase, while reach trials consisted of the 200 ms periods from the initiation of reach to food. Principal components analysis was performed on concatenated trials for each condition separately, and the dimensionality was computed by the number of principal components required to explain a 70% and 80% percent of the variance. Figure 2a and 2b show the median cumulative eigenspectra are similar for walking and reaching for both Monkey C and U, and that similar numbers of dimensions are needed to explain 70% and 80% of the total variance. These findings indicate that the power distribution and extent of coordination between neurons are similar between these two behaviors. Although the PCA eigenspectra are largely indistinguishable for swing and reach conditions, linear discriminant analysis shows that these conditions are well separated in a low-dimensional space (Fig. A1).

Lastly, we analyzed low-dimensional neural dynamics using condition-dependent PCA to describe how M1 neural structure evolves over time for these behaviors[23]. If they are consistent for a given movement, then this shows the statistical regularities of neural dynamics used to drive movement [24]. The neural state space was created using condition-dependent PCA with the swing and stance conditions, resulting in axes that describe the maximum variance accounted for that differs between swing and stance. Fig 2c and 2d shows the neural dynamics for four phases of the gait cycle (swing, midswing, stance, and midstance) and reaching, and also plots the histogram of distances from reach for each gait phase for Monkey C and U. The gait cycle has cyclic dynamics, while the reach is separate and flipped in direction from the oscillatory direction of walking. The reach trajectory is spatially closest to that of the swing phase, the most kinematically similar behavior to reach, shown in Fig. A2. Video 1 illustrates Monkey C and Monkey U neural dynamics of walking and reaching evolving through time. Taken together, our findings show that neural dynamics are different for walking and reaching despite having similar correlational structure, dimensionality, and distribution of power. This suggests that neural dynamics for these kinematically similar, yet contexually different behaviors, operate in similar subspaces but evolve differently.

This work builds on previous, partially constrained animal studies [25, 26] and establishes a freely-moving rhesus model with which to explore generalized low-dimensional motor neural dynamics. These results may be evidence for a common underlying neural structure that drives similar kinematic behaviors but traverses it differently based on context. The simplicity of a single low dimensional neural structure to perform similar behaviors suggests that motor cortex may be more bounded than theoretically thought. It highlights a potential evolutionary pressure towards a robustness of the system instead of a high dimensional noise. This understanding can place existing biological systems within their evolutionary context and reveal general principles that transcend any particular model [27]. Relating back to constrained

reaching tasks, our results suggest that low dimensional neural dynamics from a simple, constrained environment may generalize to unconstrained environments. Future work may seek to compare constrained reaching tasks to unconstrained reaching tasks to further elucidate this finding.

1 Figures

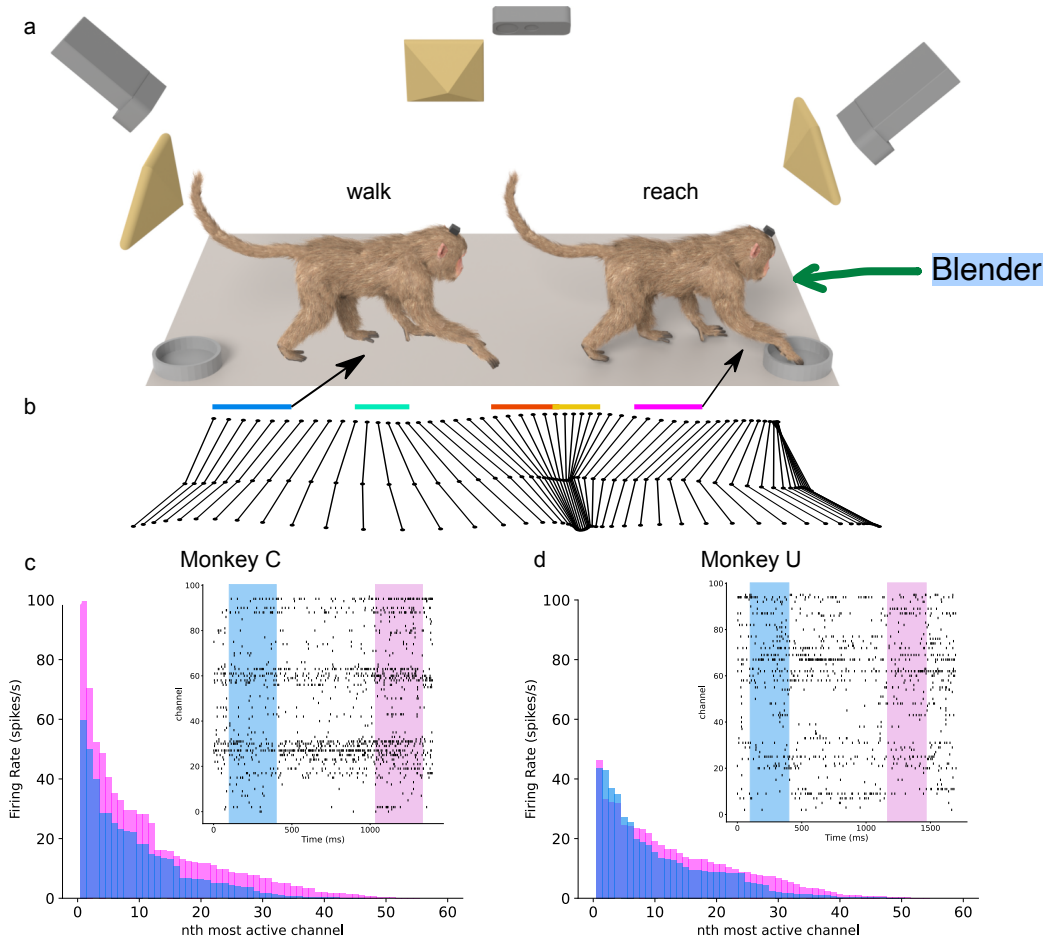

Fig. 1 Behavioral task and recorded neuronal activity. a) Diagram of the walk-reach behavioral task. The distance between the bowls is 1.5 meters. b) Continuous arm kinematics for Monkey C for one example lap. Animals take 2-3 gait phases per lap before reaching towards food in the bowl. The colored bars show 200 ms starting at the beginning of each gait phase: swing (blue), midswing (teal), stance (red), orange (midstance), and reach (magenta). The arrow from the blue bar points to the walking monkey, and the arrow from the magenta bar points to the reaching monkey to depict the two phases that have similar arm kinematics, but different complexities of movement. c) Median firing rates and raster plots for all 96 channels from M1 right arm region of Monkey C. Trial averaged firing rates using the median per channel for swing (blue) and reach (magenta) conditions. Channels were sorted from highest to lowest firing rate for each condition. Raster plot shows 1.5 seconds of data with vertical bands spanning 200 ms and color coded by trial type. d) Same as in c), but for Monkey U. The raster plot shows 2 seconds of spiking activity from the M1 left arm region.

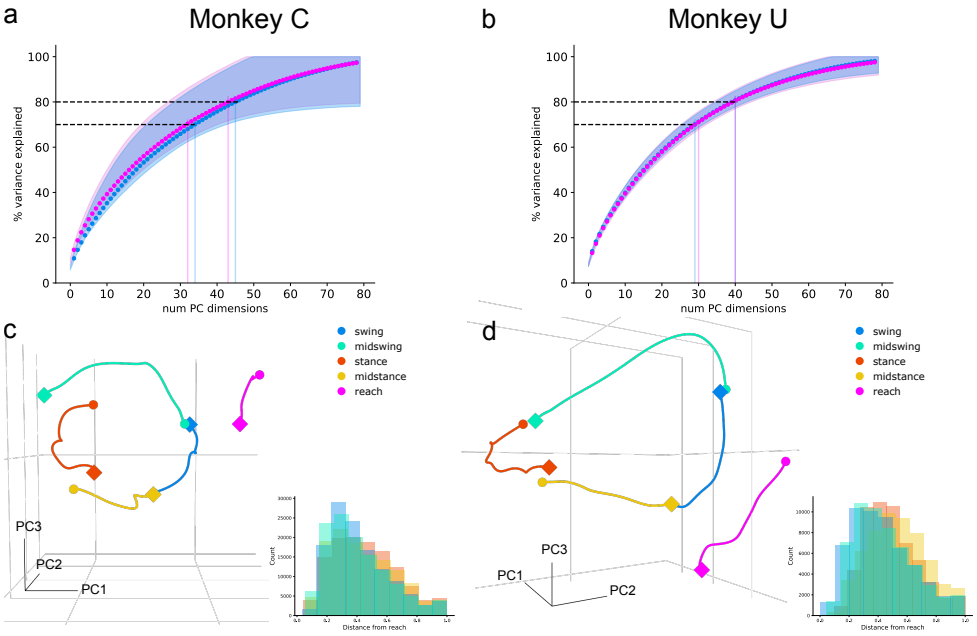

Fig. 2 Dimensionality and neuronal dynamics of unconstrained reaching and walking. The dimensionality and power distribution between reaching and walking is similar, yet neural dynamics of reaching and walking are separable. The gait cycle has oscillatory dynamics, and the reaching trajectories change in direction from that of the swing phase. a) Median and interquartile ranges across experimental days for the cumulative number of PC dimensions needed to capture a fixed percentage of variance for Monkey C. The reach condition is shown in magenta, and the swing condition is shown in blue. Vertical lines indicate the number of dimensions needed for 70% and 80% of the variance. For Monkey C, 34 and 32 dimensions for reaching and walking respectively were needed to explain 70% of the variance, and for 45 and 43 dimensions for 80% of the variance. b) Same as in a), but for Monkey U. For Monkey U, 30 dimensions for reaching and 28 dimensions for walking were needed to explain 70% of the variance, and 40 dimensions for both conditions explained 80% of the variance. c) Neural dynamics of walking and reaching in 3-d condition-dependent PC space for Monkey C. The average trajectory for all trials for each phase is plotted and color coded as defined in Fig 1b. A circle indicates the start, and a diamond indicates the end of each phase. There is a discontinuity between the midswing (teal), stance (red), and midstance (orange) phases. The swing trajectory is 270 ms, midswing is 400 ms, stance is 400 ms, midstance is 270 ms, and the reach is 200 ms. d) Same as in c), but for Monkey U. Monkey U walked slower than Monkey C, and there is less of a discontinuity between the midswing to stance phases. The swing trajectory is 320 ms, midswing is 420 ms, stance is 480 ms, midstance is 330 ms, and the reach is 300 ms. The histogram calculates the closest distance in 10-d condition-dependent PC space for each 200 ms gait phase for every point for each 200 ms reach trial. Each dimension is scaled by the fractional variance contributed, and the distance values were scaled using maximum absolute scaling. A ranksum test was performed on pairwise comparisons between swing, stance, midswing, and midstance histograms. For swing vs stance, swing vs midstance, stance vs midswing, and midswing vs midstance, $p < 0.001$ for both Monkeys C and U, showing that the swing phases are significantly closer to the reach than the stance phases.

2 Methods

Animal Procedures & Behavioral Task

All animal procedures and protocols were approved by the Stanford University Institutional Animal Care and Use Committee (IACUC). Two adult, male rhesus macaques (*Macaca mulatta*; Monkey C and Monkey U) performed an unconstrained walk and reach task. Monkey C, age 14, of Chinese origin, weighing 15.3 kg, was implanted with two 96-channel multielectrode arrays (Blackrock Microsystems, Salt Lake City, UT) in arm regions of primary motor (M1) and dorsal premotor (PMd) cortex determined by visual anatomical landmarks using standard neurosurgical techniques on March 25, 2021. Monkey U, age 12, of Indian origin, weighing 14.5 kg, was implanted with three 96-channel multielectrode arrays (Blackrock Microsystems, Salt Lake City, UT) in arm regions of primary motor (M1) and dorsal premotor (PMd) cortex determined by visual anatomical landmarks using standard neurosurgical techniques on August 4, 2017. One of the M1 arrays for Monkey U did not transmit signal, so we recorded from the other M1 array. Only M1 data was used in this analysis for both monkeys.

Months of an unconstrained reach-walk behavioral task were captured for two macaques in a large observational enclosure similar to those previously developed [28, 29]. The unconstrained behavioral task consisted of the animals walking between bowls placed on opposite sides of the enclosure and reaching for treats Laps contained different numbers of walking steps, but the average trial had two to three arm swings before the reach at the end of each lap. The reach trials were counted as valid only if the macaque maintained a standing posture on all fours. Experimental sessions and trial counts for Monkey C and Monkey U are summarized in Table 1. Animals voluntarily walked and reached for treats and were free to sit and wander around the observational space.

The gait cycle was defined by four major phases, swing, midswing, stance, and midstance for the contralateral arm. Stance periods were defined as the beginning of hand contact, swing periods were the beginning of hand lift off. Reach periods were when the animal initiated a reach for food in the bowl with the contralateral arm from the implant in M1. The beginning of stance periods and end of reach periods were hand tagged from RGB videos for the entire experimental session per day. Swing periods were extrapolated from the data as the time exactly in the middle between two stance phases. The midstance and midswing were also extrapolated as the middle time of stance the middle time of swing respectively.

Neural data processing

Neural data were recorded in M1 cortical arm region from Blackrock Inc. Cereplex W. These signals were acquired at 30 kHz. However, due to the unconstrained nature of our study and wireless transmission of our recording device, there were more artifact in the form of motion artifact, static, and drops in our neural recordings than in unconstrained studies. Therefore, high pass filtering and thresholding to detect spikes were not sufficient to detect true spikes. We filtered the true spikes from the artifact

by using cross correlating potential spikes with a wavelet template taken from our constrained rig and also filtered based on the biological size of the depolarization.

Data collected from the Cereplex W contained artifact due to static and drops in the data. This artifact was removed by taking a rolling root mean square (RMS) of 100 sample intervals for the entire neural high pass filtered data for that day. Drops in the data had an RMS of less than 5 μV and very large changes due to static causing voltages to sharply max out were and RMS above 70 μV. Neural data was counted as valid if the RMS was between 5 and 70 μV. Data with an RMS value less than 5 or greater than 70, was not included in our subsequent thresholding. We then took the RMS of 60 seconds of valid data for each channel and multiplied by a factor of -4 to obtain a per channel threshold [30]. Thresholds were around -40 to -50 μV.

Smaller artifact due to movement of the head and body passed threshold detection, so an additional spike filtering algorithm was used to sort the artifact from spikes. We performed a cross correlation between any detected spike and wavelet template taken from the same array in a constrained rig. We counted a potential spike as true if the cross correlation peak was around 47-48 samples, ensuring that the depolarization was in the correct spatial location. Additionally, physiologically the depolarization of a spike should last less than 200 ms which is about 10 samples. We found the minimum of the spike and found the two inflection points around the minimum. We counted the number of samples the depolarization lasted, and if the number was between 7 and 14 samples, we counted it as a true spike.

After the additional spike filtering, a 30kHz raster was constructed from the filtered neural data and then downsampled into a 1kHz raster. Finally, to remove any remaining array-wide artifact, spikes that showed up on more than 30 channels (1/3 of the array) within the same millisecond were removed.

Synchronization of neural and behavioral data

Neural data are transmitted from the animal through a wireless headstage (CerePlex W, Blackrock Microsystems, Salt Lake City, UT). Outside the enclosure, 16 panel antennas (PA-333810-NF 3.3GHz-3.8GHz 10dBi Panel Directional Outdoor Antenna, FT-RF, Jhubei City, Taiwan) are evenly spaced to receive signals from two wireless headstages operating at distinct frequencies in the 3-4 GHz range. This allows hundreds of channels of neural data to be simultaneous recorded. Raw neural data were sampled at 30 kHz and saved to a SQLite database. At this sampling frequency, 192 channels generates a data rate of approximately megabytes per second.

The neural data was collected from a neural acquisition system and the behavioral data was collected from four RGB-D Microsoft Azure Kinects at 30Hz. The four cameras were synced to each other using a master camera that controlled when the other cameras shutters went off. The cameras were asynchornously triggered by the neural acquisition system. Three square LED lights were placed outside of the observational enclosure on the three sides that did not include the tunnel entrance. The status of the light (on or off) appeared in the RGB frames. We used the binary status of the light to encode the frame number. The sequence of lights created a continuous binary stream with an 8 number header of 1,1,1,0,0,1,1,0 to signify a starting frame.

Low-dimensional linear analysis

The mathematical modeling of simultaneous multi-neuron activity involves dimensionality reduction to linearly map 10^2 neurons to a 10-20 dimensional state space comprised of these projection axes. This low-dimensional state space is termed the neural state, which corresponds to coordinated action potential firing rates of the recorded neurons. The evolution of the neural state space over time is termed low-dimensional neural dynamics (LDND). The simplest, input-free linear example of LDND is of the form:

$$\frac{dx}{dt} = Ax \tag{1}$$

where x is the 10-20 dimensional neural population state and A is the dynamical update matrix. There are multiple different methods of performing dimensionality reduction and forming linear low-dimensional neural dynamics. We perform three main dimensionality reduction techniques, principal component analysis (PCA), condition-dependent PCA, and linear discriminant analysis (LDA).

2.1 PCA

Principal component analysis is a linear dimensionality reduction tool that preserves variance between the latent variables it finds. In the context of neural data, it maps neural firing rates into principal components (PCs), where the top PCs capture the most amount of variance within the data. Each PC axis minimizes the distance between the original points and their projections. PCA was performed on concatenated multiple trials of data for the same event type, and the latent spaces includes complex dependencies on stimulus and time. PCA is an unsupervised mathematical model of the data because there are no labels given when the algorithm is fitting the data to projection axes. We performed PCA on hundreds of trials collected over multiple days to construct to separate eigenspectra for the swing and reach conditions.

PCA was performed separately on concatenated 200 ms trials for the swing and reach conditions, creating two different subspaces for each experimental day. The same number of swing and reach trials were included for each experimental day. Trials were created by applying a Gaussian kernel with a 30 ms standard deviation to a raster of 500 ms before and 500 ms after the start of each trial to create smoothed firing rates for all 96 channels.

2.2 Condition-dependent PCA

We used condition dependent PCA, a more supervised linear model that incorporates trial type information, to construct the neural state space that represents largest difference between the swing and stance conditions [31]. Briefly, we subtract the overall mean (denoted by $< . >$ firing rate of the neurons of all neurons and all trials r_{all} , giving us a scalar $\bar{x}$:

$$\bar{x} =< r_{all} > \tag{2}$$

We then find the condition independent firing rate for each channel, which is the mean of the firing rates across all trials of the all conditions $r_{allcond}$ minus the mean firing

rate:

$$x_{ind} =< r_{allcond} - \bar{x} > \tag{3}$$

Finally, the condition dependent part is the firing rate across all trials for the same condition minus the condition independent part.

$$x_{dep} =< r_{onecond} - x_{ind} > \tag{4}$$

We concatenated 200 ms condition dependent arrays for swing and stance and performed PCA on this condition dependent data. Swing and stance trials were created by binning and summing every 30 ms for the 200 ms raster for each of the 96 channels. The resulting output is the projection axes that describe the maximum variance accounted for that differs between swing and stance. We then plotted all trials for all four gait phases (swing, stance, midswing, and midstance) and reaches in the swing-stance PCA subspace. Trial times for the four gait phases varied so that the end of each phase would line up with the beginning of the subsequent one. The median of each of the four gait phases were plotted for the neural trajectories.

2.3 Linear discriminant analysis

We performed linear discriminant analysis between the reach and swing conditions to find the projection that optimally separates these two conditions. The same number 200 ms trials were concatenated for the swing and reach conditions for each experimental day. Trials were created by binning and summing every 30 ms for the 200 ms raster for each of the 96 channels. Swing trials were labelled as -1 and reach trials were labelled as 4. LDA was performed on all trials to create a linear decision boundary and decision function. Linear discriminant analysis computes the largest hyperplane between the two scenarios by maping the firing rates of neurons onto one latent space that represents the largest separation between two conditions while preserving the geometry of the neural activity. LDA is a linear classification machine learning algorithm that creates a probabilistic model per class based on the specific distribution of observations for each input variable. It is the most supervised approach, because we provide labels of each condition to calculate the conditional probability of a new trial belonging to one of the conditions.

3 Supplementary information

Fig. 1 Behavioral task and neural activity comparing unconstrained reaching and walking.

Fig. 2 Dimensionality and neural dynamics of unconstrained reaching vs. and unconstrained walking.

Table A1 Trial counts for Monkey C and Monkey U.

Fig. A1 Neural activity for unconstrained reaching and unconstrained walking are separable in both LDA state space and dynamics.

Fig. A2 Distance from the median reach phase to the four median gait phases, swing, midswing, stance, and midstance.

Fig. A3 Neural trajectories from three different angles.

Additional supp figs that I will do

- raction of variance each gait phase + reach explains variance in each gait phase
- Fig2 c and d do same analysis for 40 / 96 dimensions - small dimensions don't change the distance
- quantify fraction of flip of trajectories, flow field
- dynamics with all of the data: dpca
- dynamics with all of the data: regular pca

Nonauthor Contributors M. Wechsler, and M. Risch were responsible for animal care and surgical support. S.I. Ryu was responsible for non-human primate array implantation. I.E. Bray assisted in animal care.

Acknowledgments: We thank K. Chin and M. Truong for administrative support. P. Nuyujukian's affiliations are Bioengineering, Neurosurgery, Electrical Engineering, Wu Tsai Neurosciences Institute, Stanford Bio-X; Stanford University. **Funding**:

Author Contributions: ASL and MPS were responsible for collecting data with Monkey C (investigation). ASL and SEC and EJJ were responsible for collecting data with Monkey U (investigation). MPS was responsible for developing the data capture pipeline which recorded from cameras (methodology, software). ASL was responsible for developing the neural data filtering and synchronizing neural data (methodology). ASL was responsible for performing all analysis (formal analysis). Data curation and data visualization were performed by ASL. ASL wrote the original draft, reviewed, and edited the manuscript. PN was involved in all aspects of the project, conceptualized the work, supervised the effort, provided funding, and reviewed and edited the manuscript. **Competing interests**: The authors have no competing interests. **Data and materials availability**: All data needed to evaluate the conclusions in the paper are present in the paper or the Supplementary Materials.

Appendix A Supplementary

Monkey C	Reach trials	Monkey U	Reach trials
C220405_01	16	U221130_01	26
C220406_01	31	U221201_01	46
C220407_01	24	U221202_01	63
C220411_01	82	U221205_01	61
C220414_01	160	U221206_01	72
C220418_01	110	U221215_01	96
C220419_01	156	-	-
C220422_01	136	-	-
C220804_01	10	-	-

Table A1 Experimental sessions and trial counts for Monkey C and Monkey U. Analysis for reach and swing were trial matched to the number of reaches from the contralateral arm for each day. Monkey C had 9 experimental days, and 725 reach and swing trials total from his right arm. Monkey U had 6 experimental days, and 364 reach and swing trials total from his left arm.

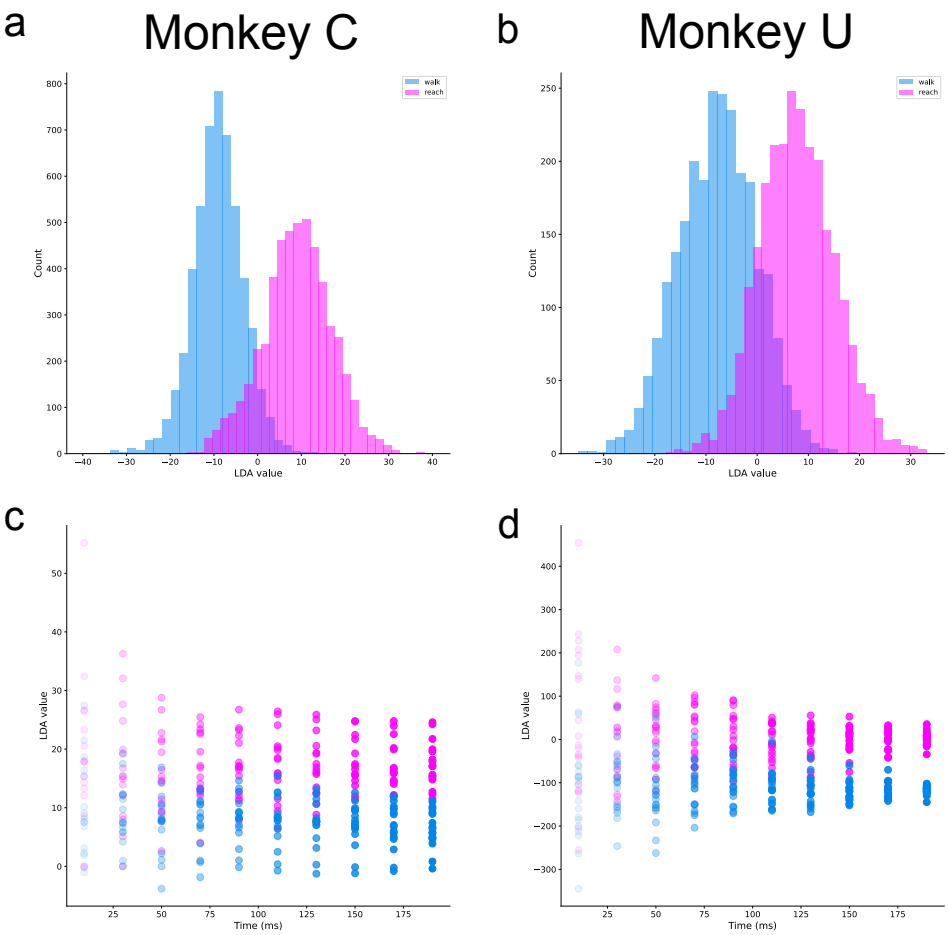

Fig. A1 Neural activity for unconstrained reaching and unconstrained walking are separable in both LDA state space and dynamics. LDA finds an axis that best separates neural activity for 200 ms trials unconstrained reaching and unconstrained walking. a) LDA histogram for Monkey C showing a clear separation between the two conditions. b) LDA histogram for Monkey U. c) LDA trajectories for Monkey C. Trajectories were predicted using the linear decision boundary to classify unlabeled trials of 10 up to 200 ms bins every 20 ms, and plotted either magenta for reach or blue for swing as a function of the time bin. d) Same as in c) but for Monkey U.

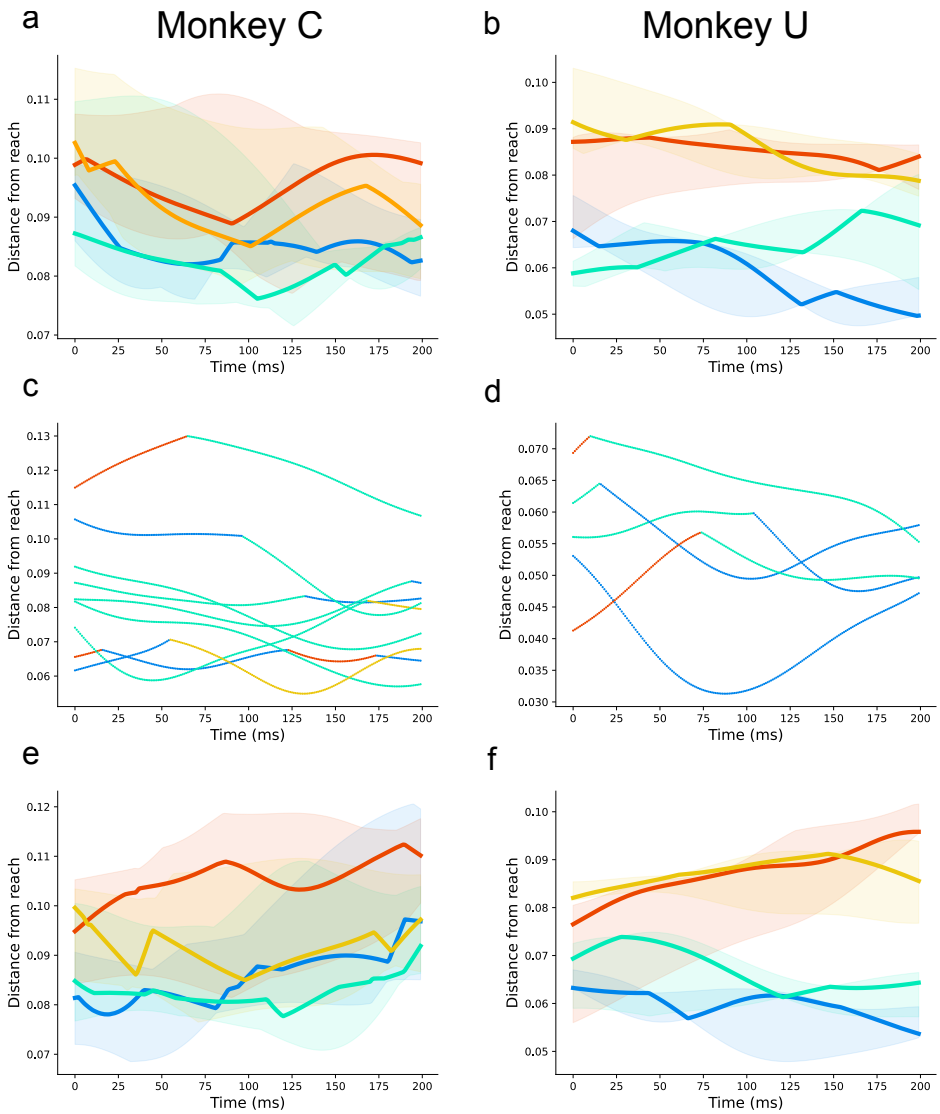

Fig. A2 Distance from the median reach phase to the four median gait phases, swing (blue), midswing (teal), stance (red), and midstance (orange). a) Median distance from 0-200 ms of each gait phase to 0-200 ms of the reach for each experimental day. Shadowing shows the interquartile ranges. b) Same as in a) but for Monkey U. c) The closest median individual phase to each point of 0-200 ms median reach phase. Each line is a different experimental day. d) Same as in c) but for Monkey U. e) Median distance from 0-200 ms of each gait phase to the reversed reach (200-0 ms) for each experimental day. Shadowing shows the interquartile ranges. f) Same as in e) but for Monkey U.

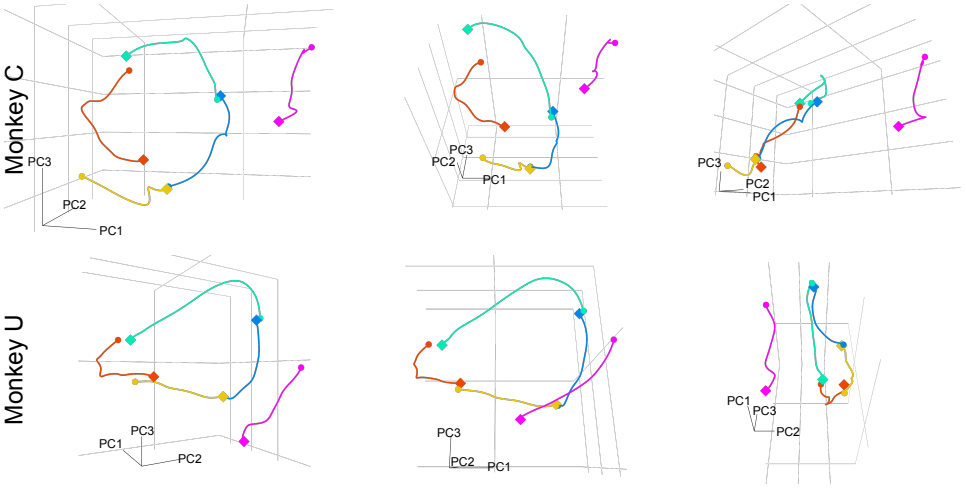

Fig. A3 Neural dynamics trajectories in different angles. The first panel shows the dynamics view from Fig 2c and 2d for Monkey C and U. The second panel shows the angle at which the area of the circular gait trajectory is maximally projected onto a plane. The third panel shows the angle at which the swing phase and reach phase are maximally separated.

References

[1] Churchland, M.M., Cunningham, J.P., Kaufman, M.T., Foster, J.D., Nuyujukian, P., Ryu, S.I., Shenoy, K.V.: Neural population dynamics during reaching. Nature **487**(7405), 51–56 (2012)

[2] Scott, B.B., Constantinople, C.M., Akrami, A., Hanks, T.D., Brody, C.D., Tank, D.W.: Fronto-parietal Cortical Circuits Encode Accumulated Evidence with a Diversity of Timescales. Neuron **95**(2), 385–398 (2017) https://doi.org/10.1016/j.neuron.2017.06.013

[3] Brewer, A.A., Barton, B.: Maps of the Auditory Cortex. Annu Rev Neurosci **39**, 385–407 (2016) https://doi.org/10.1146/annurev-neuro-070815-014045

[4] Aflalo, T., Kellis, S., Klaes, C., Lee, B., Shi, Y., Pejsa, K., Shanfield, K., Hayes-Jackson, S., Aisen, M., Heck, C., Liu, C., Andersen, R.A.: Neurophysiology. Decoding motor imagery from the posterior parietal cortex of a tetraplegic human. Science **348**(6237), 906–910 (2015) https://doi.org/10.1126/science.aaa5417

[5] Pandarinath, C., Gilja, V., Blabe, C.H., Nuyujukian, P., Sarma, A.A., Sorice, B.L., Eskandar, E.N., Hochberg, L.R., Henderson, J.M., Shenoy, K.V.: Neural population dynamics in human motor cortex during movements in people with als. Elife **4** (2015) https://doi.org/10.7554/eLife.07436

[6] Yu, B.M., Cunningham, J.P., Santhanam, G., Ryu, S.I., Shenoy, K.V., Sahani, M.: Gaussian-Process Factor Analysis for Low-Dimensional Single-Trial Analysis of Neural Population Activity. Journal of Neurophysiology **102**(1), 614–635 (2009) https://doi.org/10.1152/jn.90941.2008

[7] Kao, J.C., Nuyujukian, P., Ryu, S.I., Churchland, M.M., Cunningham, J.P., Shenoy, K.V.: Single-trial dynamics of motor cortex and their applications to brain-machine interfaces. Nat Commun **6**, 7759 (2015) https://doi.org/10.1038/ncomms8759

[8] Kaufman, M.T., Seely, J.S., Sussillo, D., Ryu, S.I., Shenoy, K.V., Churchland, M.M.: The Largest Response Component in the Motor Cortex Reflects Movement Timing but Not Movement Type. eNeuro **3**(4) (2016) https://doi.org/10.1523/ENEURO.0085-16.2016

[9] Sadtler, P.T., Quick, K.M., Golub, M.D., Chase, S.M., Ryu, S.I., Tyler-Kabara, E.C., Yu, B.M., Batista, A.P.: Neural constraints on learning. Nature **512**(7515), 423–426 (2014) https://doi.org/10.1038/nature13665

[10] Golub, M.D., Sadtler, P.T., Oby, E.R., Quick, K.M., Ryu, S.I., Tyler-Kabara, E.C., Batista, A.P., Chase, S.M., Yu, B.M.: Learning by neural reassociation. Nature neuroscience **21**(4), 607–616 (2018) https://doi.org/10.1038/s41593-018-0095-3

[11] Hennig, J.A., Golub, M.D., Lund, P.J., Sadtler, P.T., Oby, E.R., Quick, K.M., Ryu, S.I., Tyler-Kabara, E.C., Batista, A.P., Yu, B.M., Chase, S.M.: Constraints on neural redundancy. Elife **7** (2018) https://doi.org/10.7554/eLife.36774

[12] Shenoy, K.V., Sahani, M., Churchland, M.M.: Cortical Control of Arm Movements: A Dynamical Systems Perspective. Annual Review of Neuroscience **36**(1), 337–359 (2013) https://doi.org/10.1146/annurev-neuro-062111-150509

[13] Rouse, A.G., Schieber, M.H.: Condition-Dependent Neural Dimensions Progressively Shift during Reach to Grasp. Cell Reports **25**(11), 3158–3168 (2018) https://doi.org/10.1016/j.celrep.2018.11.057

[14] Pandarinath, C., Gilja, V., Blabe, C.H., Nuyujukian, P., Sarma, A.A., Sorice, B.L., Eskandar, E.N., Hochberg, L.R., Henderson, J.M., Shenoy, K.V.: Neural population dynamics in human motor cortex during movements in people with ALS. eLife **4**(JUNE) (2015) https://doi.org/10.7554/eLife.07436

[15] Willett, F.R., Deo, D.R., Avansino, D.T., Rezaii, P., Hochberg, L.R., Henderson, J.M., Shenoy, K.V.: Hand Knob Area of Premotor Cortex Represents the Whole Body in a Compositional Way. Cell **181**(2), 396–409 (2020)

[16] Sompolinsky, H.: Computational neuroscience: beyond the local circuit. Current opinion in neurobiology **25**, (2014)

[17] Gao, P., Ganguli, S.: On simplicity and complexity in the brave new world of large-scale neuroscience. Current opinion in neurobiology **32**, 148–155 (2015)

[18] Foster, J.D., Nuyujukian, P., Freifeld, O., Ryu, S.I., Black, M.J., Shenoy, K.V.: A framework for relating neural activity to freely moving behavior. In: Proceedings of the Annual International Conference of the IEEE Engineering in Medicine and Biology Society, EMBS (2012). https://doi.org/10.1109/EMBC.2012.6346530

[19] Foster, J.D., Nuyujukian, P., Freifeld, O., Gao, H., Walker, R., Ryu, S.I., Meng, T.H., Murmann, B., Black, M.J., Shenoy, K.V.: A freely-moving monkey treadmill model. Journal of Neural Engineering **11**(4) (2014) https://doi.org/10.1088/1741-2560/11/4/046020

[20] Borton, D.A., Y, M., Aceros, J., Nurmikko, A.: An implantable wireless neural interface for recording cortical circuit dynamics in moving primates. J of Neural Eng **10**(2), 26010 (2013)

[21] Xing, D., Aghagolzadeh, M., Truccolo, W., Borton, D.: Low-Dimensional Motor Cortex Dynamics Preserve Kinematics Information During Unconstrained Locomotion in Nonhuman Primates. Frontiers in neuroscience **13**, 1046 (2019) https://doi.org/10.3389/fnins.2019.01046

[22] Silvernagel, M.P., Ling, A.S., Nuyujukian, P., Laboratory, B.I.: A markerless

platform for ambulatory systems neuroscience. Science Robotics **6**(58), 7045 (2021)

[23] Churchland, M.M., Cunningham, J.P., Kaufman, M.T., Foster, J.D., Nuyujukian, P., Ryu, S.I., Shenoy, K.V.: Neural population dynamics during reaching. Nature **487**(7405), 51–56 (2012)

[24] Yu, B.M., Kemere, C., Santhanam, G., Afshar, A., Ryu, S.I., Meng, T.H., Sahani, M., Shenoy, K.V.: Mixture of Trajectory Models for Neural Decoding of Goal-Directed Movements. J Neurophysiol **97**, 3763–3780 (2007)

[25] Foster, J.D., Freifeld, O., Nuyujukian, P., Ryu, S.I., Black, M.J., Shenoy, K.V.: Combining wireless neural recording and video capture for the analysis of natural gait. In: 2011 5th International IEEE/EMBS Conference on Neural Engineering, pp. 613–616 (2011). IEEE

[26] Foster, J.D., Nuyujukian, P., Freifeld, O., Gao, H., Walker, R., Ryu, S.I., Meng, T.H., Murmann, B., Black, M.J., Shenoy, K.V.: A freely-moving monkey treadmill model. Journal of neural engineering **11**(4), 046020 (2014)

[27] Gao, P., Ganguli, S.: On simplicity and complexity in the brave new world of large-scale neuroscience. Current opinion in neurobiology **32**, 148–155 (2015)

[28] Silvernagel, M.P., Ling, A.S., Nuyujukian, P., Laboratory, B.I.: A markerless platform for ambulatory systems neuroscience. Science Robotics **6**(58), 7045 (2021)

[29] Bala, P.C., Eisenreich, B.R., Yoo, S.B.M., Hayden, B.Y., Park, H.S., Zimmermann, J.: Automated markerless pose estimation in freely moving macaques with openmonkeystudio. Nature communications **11**(1), 1–12 (2020)

[30] Chestek, C.A., Gilja, V., Nuyujukian, P., Kier, R.J., Solzbacher, F., Ryu, S.I., Harrison, R.R., Shenoy, K.V.: HermesC: low-power wireless neural recording system for freely moving primates. IEEE Transactions on Neural Systems and Rehabilitation Engineering **17**(4), 330–338 (2009)

[31] Kobak, D., Brendel, W., Constantinidis, C., Feierstein, C.E., Kepecs, A., Mainen, Z.F., Qi, X.-L., Romo, R., Uchida, N., Machens, C.K.: Demixed principal component analysis of neural population data https://doi.org/10.7554/eLife.10989.001